Applied Energy 208 (2017) 83–96

Contents lists available at ScienceDirect

Applied Energy

journal homepage: www.elsevier.com/locate/apenergy

Spectral selective and photothermal nano structured thin films for energy efficient windows

Julian (Jialiang) Wang[a,b], Donglu Shi[c,d,*]

[a] Department of Civil and Architectural Engineering and Construction Management, College of Engineering and Applied Science, University of Cincinnati, Cincinnati, OH 45221-0012, United States
[b] School of Architecture and Interior Design, College of Design, Architecture, Art, and Planning, University of Cincinnati, Cincinnati, OH 45221-0016, United States
[c] The Institute for Translational Nanomedicine, Shanghai East Hospital, the Institute for Biomedical Engineering & Nano Science, Tongji University School of Medicine, Shanghai 200092, China
[d] The Materials Science and Engineering Program, College of Engineering and Applied Science, University of Cincinnati, Cincinnati, OH 45221, USA

HIGHLIGHTS

- Identified the critical issues and ideal models in window thin film designs.
- Applied the novel photothermal nano coatings to windows for the first time.
- A new design of window structure is proposed for energy-efficient windows.

ARTICLE INFO

Keywords:
Energy savings
Building windows
Thin films
Photothermal
Nanoparticles

ABSTRACT

This review deals with critical issues in the development of energy-efficient windows from two fundamentally different approaches, namely, spectral selectivity and photothermal effect. This review is therefore divided into two parts. The first part reviews the engineering considerations based on an ideal window concept in terms of spectral selectivity, glazing scale, seasonal factors, and related thermal transfer. In particular, spectrally selective window designs and metal-based thin films are introduced with optimized engineering parameters and physical properties. The second part introduces a new approach of thermal insulation via the photothermal effect of the nanostructured thin films and coatings. The key that limits the heat flow through windows is the thermal insulation, which is traditionally constructed by multi-pane structures with an insulating layer. A novel concept not relying on any insulating media, but photothermal effects of nanomaterial coatings has been recently proposed and experimental verified. Both concepts of spectral selectivity and photothermal effects are introduced for energy-efficient window applications. A new direction is proposed in the development of the energy-efficient windows via the photothermal effects in various nanostructures of thin films and coatings.

1. Introduction

Windows are one of the most important building envelope components, due to their large areas with required thermal and optical performances. The U.S. Department of Energy (DOE) has reported that the heat loss through windows in cold weather is approximately 3.95 quads (or 1.16 e + 12 kWh) of primary energy use in the U.S. based on the statistical data by the 2016 SHIELD program [1]. Preventing heat flow of this type has presented great challenges to both civil/architectural engineers and material/chemical scientists for collaboratively developing more energy efficient structures. Heat transfer through a window occurs via conduction, convection, and radiation. A parameter used to characterize the overall heat transfer rate or insulation capability of a window assembly is the so-called U-factor, which combines the effects of three types of aforementioned heat transfer. A low U-factor indicates a high insulation ability or low heat transfer through a window. The current methods in developing windows with low U-factors are mainly from two directions: structural and spectral designs.

In current structural design, multi-plane glazing is the most popular approach that focuses primarily on conductive heat transfer. Such a structure normally consists of two or more glass panes separated by insulating layers of air, inert gas, vacuum cavities, phase changed materials, silica aerogel, or some dynamic controls, such as airflow or water flow [2–10]. The materials that can serve as transparent thermal

* Corresponding author at: The Materials Science and Engineering Program, College of Engineering and Applied Science, University of Cincinnati, Cincinnati, OH 45221, USA.
E-mail address: donglu.shi@uc.edu (D. Shi).

http://dx.doi.org/10.1016/j.apenergy.2017.10.066
Received 2 August 2017; Received in revised form 10 October 2017; Accepted 18 October 2017

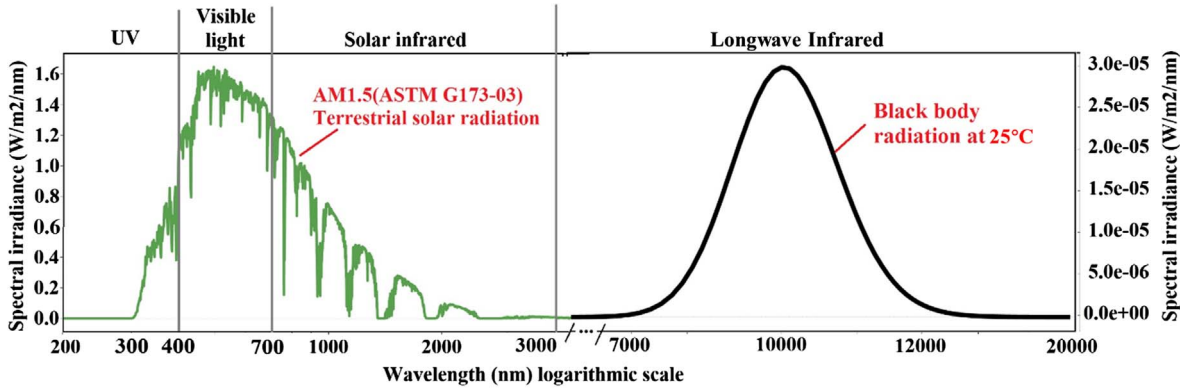

Fig. 1. Standard terrestrial reference spectrum and black body spectra at 25 °C (It is calculated from Planck's Law).

barriers are therefore sought with low thermal conductivity and good visible light transmission. Spectral design mainly deals with radiative heat transfer for energy efficient windows, normally through thin films, tints, or coatings that respond to surrounding thermal radiations. For temperatures of practical interest in the building energy studies, thermal radiation flux occurs in four basic bands: ultraviolet radiation ($100\,nm < \lambda < 400\,nm$), visible light ($400\,nm < \lambda < 700\,nm$), and solar infrared radiation ($700\,nm < \lambda < 3000\,nm$) from the sun, and longwave radiation ($3000\,nm < \lambda < 50{,}000\,nm$) from the building interior or outdoor environmental temperatures (see Fig. 1). Regulating window transmission, absorption, and reflection properties to control the passage of thermal radiation in these ranges can significantly improve building energy efficiency. Typical conventional technologies include spectrally selective films, anti-reflection films, chromic technologies (e.g., electrochromic, thermochromic, and photochromic materials), angular selective coatings, liquid crystals, and electrophoretic or suspended-particle technologies. These glazing technologies are commonly preferred and used by architects for their strong impacts on building energy efficiency, indoor thermal and visual comfort, façade appearance, and architectural aesthetics. Despite of considerable progresses made in the glazing technologies, challenges remain that limit further optimization of energy efficiency. These include independent multispectral band modulations and unidirectional transparency of infrared thermal radiations. The purpose of this paper is to review representative concurrent spectral selective energy efficient window film designs and trace their fundamental features, and then introduce a recent novel approach in increasing window thermal insulation based on photothermal effect of nanoparticles.

This review is structurally composed of two parts, and respectively dealing with critical issues in developing energy-efficient window structures from two fundamentally different technical approaches – spectral selectivity and photothermal effects. In Part I, we first provide a brief discussion on the fundamental aspects of ideal windows as a baseline for engineering considerations and thin-film technologies. Based on a perfect window, materials structural design is possible in order to simulate these ideal properties. Various approaches will be introduced for this purpose including thin film low-e coatings, modulating of transmission and/or reflection for controlled thermal radiation fluxes, and spectrally selective structures for optimum optical features. We then extend the ideal window concept to the fundamental requirements and strategies of spectrally selective thin film design. The most representative benchmark examples and their optical performance are subsequently introduced in terms of transmittance in visible and infrared regions. In particular, selective absorption properties in designated photon frequency regions can now be tuned via nanostructures, materials compositions, and externally applied electrical field (smart materials) [11–13].

It is pointed out in this review, however, despite of the current window technologies aforementioned, major challenges cannot be easily addressed for further optimization of energy efficiency. Limited by the intrinsic materials properties, development of ideal windows still faces great challenges in both materials synthesis, thin film architecture, and engineering design. To address these critical issues, we introduce a recently developed novel approach fundamentally different from the spectral selectivity, namely, photothermal effect through design of new nano structures. In this unique approach, energy efficiency is achieved via the photon-activated heating processes in the nanomaterials, which is the core mechanism in the design of the new thin film structures for window applications.

The second part of the review introduces a new design of window structure with significantly reduced heat loss based on the photothermal effects of nanomaterials. It should be particularly noted that although the photothermal effects have been discovered and extensively studied for metallic nanoparticles, such as gold, for medical therapeutics, few has been carried out in the deposition of thin films and window coatings for energy applications. In fact, the research on the photothermal thin films and coatings has just begun very recently, but the initial work has paved a new path in the development of energy-efficient materials in a viable and economic fashion. In particular, the photothermal effects of the Fe_3O_4 nanoparticles are discussed in terms of nanostructures, defects, fundamental mechanisms responsible for photothermal heating, and the balance between photon transmission and photothermal conversion efficiency. The so-called photothermal effect of nanoparticles is utilized to reduce the center-of-glass U-factor by slightly heating up the window interior surfaces under solar irradiation. Engineering parameter calculations such as photothermal conversion efficiency and center-of-glass U-factor are also provided for window designs. From the energy saving perspective, we address the critical issues of selective absorption of solar-infrared radiation and thermal energy convert efficiency for overall window performance in cold climate. We will finally conclude on both conventional spectral selective and new photothermal thin-film designs that are tailored to the energy requirements.

2. Part I window designs based on spectral selectivity

2.1. Basic concept

The thermal properties of a window, such as the U-factor, solar heat gain coefficient (SHGC), are understood as the essential indicators of window energy performances. Light transmittance (VT) and haze level (h) are particularly important window function parameters that characterize the visual contact with the outside world. To achieve high optical and thermal performances, the concept of a "perfect window" or "ideal window" has been developed [14,15]. Fig. 2 shows the schematic diagrams of the perfect window models.

As is well-known, the visible solar spectrum is considered essential to occupants (e.g., for their well-being, health, work efficiency, etc.)

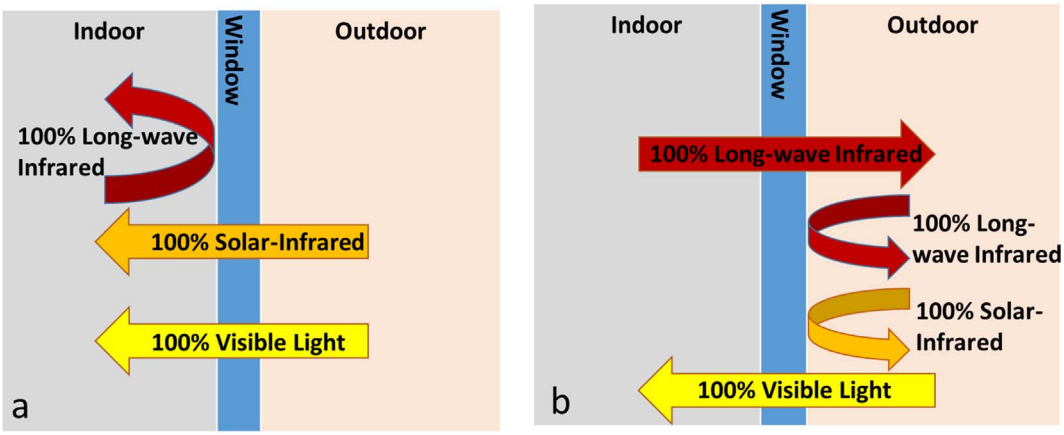

Fig. 2. Schematic diagrams showing the perfect window models for (a) winter and (b) summer.

and useful for other forms of energy such as electric light [16–20]. A perfect window should therefore permit high visible light transmission (VT) from the complete solar spectrum. Regarding thermal aspect, a perfect window should be able to seasonally control all types of radiative emissions for minimum energy consumption and reasonable indoor comfort, as environmental radiation changes in summer and winter (outdoor solar radiation and interior longwave thermal radiation). In the winter season (Fig. 2a), a perfect window needs to be completely transparent to incoming visible and infrared radiations and reflect all longwave radiation flux back to the interior for energy saving. In the summer season (Fig. 2b), a perfect window should reflect 100% solar-infrared radiations from the sun and any longwave thermal radiation from external environment. In addition, the perfect window has to maintain the unidirectional transparency to allow emissions of longwave thermal radiations from building interior to exterior.

Based on the concept of perfect window, thin films are designed and develop to simulate these ideal properties, so that their transmission and/or reflection features are regulated for selected and controlled passages of thermal radiation fluxes. However, limited by the intrinsic materials properties, development of ideal windows still faces great challenges in both materials synthesis, thin film architecture, and engineering design. Current nanotechnology has shed new light on completely different ways of solving these engineering problems from perspectives of thermal insulation, spectral selectivity, and multilayer film deposition [21–23]. In particular, selective absorption properties in designated photon frequency regions can now be tuned via nanostructures, materials compositions, and externally applied electrical field (smart materials) [11–13].

2.2. Spectrally selective thin films

Spectrally selective design aims at permitting particularly selected portions of the light spectrum to pass through a medium, while blocking others. This function is conventionally achieved in the glazing applications via highly-doped conducting/semiconducting materials and metal-based films. On the one hand, one way of solar heat control is through reflecting the heat from the sun mainly near IR. The Indium tin oxide (ITO) and fluorine-doped tin oxide (FTO) are extensively studied with dopants such as Zn, In, and Sn, that enhance IR reflectivity. However, the dopant level can only reach certain limits from the synthesis perspective, and further doping is not without considerable difficulties [24]. On the other hand, if the metal-based films with Ag, Cu, Au, or Al are made sufficiently thin (smaller than wavelength), their visible light transmittance is well enhanced but with strong IR reflection [25]. However, durability of these single-metal films has been an issue when exposed to the atmosphere [26]. Multilayer thin films with a structure of dielectric/metal/dielectric (D/M/D) have therefore been proposed and developed for building fenestration. Presently, most of the high-performance D/M/D thin films are based on ultra-thin silver film, sandwiched between two dielectric or metal oxide layers, such as Zinc oxide (ZnO), FTO, Titanium dioxide (TiO_2), and aluminum-doped zinc oxide (AZO) [27–30]. Refraction takes place as light travels from one optical medium to another. Some portion of the light is reflected at the interface between the two media with an angle relative to the surface and incoming light. Two reflected light waves will interfere, and their phase (ϕ) difference determine the degree of constructive (two reflected waves are in-phase $\phi = 0$) or destructive interferences (two reflected beams have opposite-phase $\phi = 180$). Consequently, by a proper design of each layer thickness, the destructive optical interference may enhance visible transmittance, while maintaining considerable reflectance of longwave due to the metallic layer. Furthermore, these thin films can be stacked multiply up to hundred layers for optimum visible transparency and longwave reflectance [31]. For instance, adding more pairs of sub-10 nm silver layers between high refractive index oxide layers results in sharp curves and divisions between the visible region (70% transmittance at about 700 nm) and IR region (10% transmittance at about 800 nm) [32]. The techniques for making these metal-based spectrally selective thin films include chemical vapor deposition, physical vapor deposition, thermal evaporation, and plasma ion assisted deposition [33–36]. It has been reported that coatings deposited using chemical vapor deposition technique can lead to more durable and better spectrally selective coatings [37].

In order to compare the metal-based spectrally selective thin films with the perfect window model, we plot various spectral curves of thin films including those of the perfect window using simulation by Window Optics 6 [38], as shown in Fig. 3. In Fig. 3a, for heating- and cooling-dominated climates, two idealized thin films are presented: Type A is characterized by $T = 1$, $R = 0$ (T and R respectively denote transmittance and reflectance) for $400 < \lambda < 700$ nm, and $T = 0$ for $700\text{ nm} < \lambda < 50{,}000$ nm. For Type B, the parameters are set at: $T = 1$, $R = 0$ for $400 < \lambda < 3{,}000$ nm, and $T = 0$ for $3000 < \lambda < 50{,}000$ nm. SHGC is normally used to guide the selection of glazing systems in different weathers [39]. The high-SHGC low-e coatings are commonly used in cold weather conditions, while the low-SHGC low-e coatings for warm weather climates.

Fig. 3b and c presents the spectral curves of reflectance, transmission, and absorption of two as-deposited thin films on a single glass. By comparing with the idealized spectra shown in Fig. 3a, the low-SHGC low-e coating (e.g. triple silver unit) in Fig. 3b exhibits behaviors similar to that of Type A for minimum IR transmission in hot climates. Fig. 4a shows the schematic diagram of the low-SHGC low-e coating with typical optical properties. As shown in this figure, the low-e coating is able to reflect over 90% of solar infrared and longwave infrared and still transmit 61% visible light. The key in this category is to

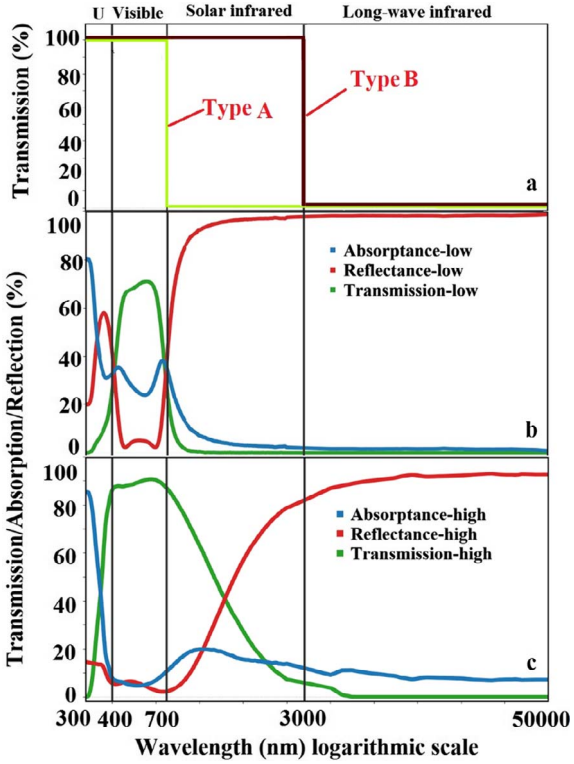

Fig. 3. (a) Idealized coatings: Type A and Type B is characterized by transmittance in specific wavebands and ideally for summer and winter, respectively. (b) Spectra of low-SHGC low-e coatings, SHGC = 0.26, VT = 0.70, Emissivity = 0.02. (c) Spectra of high-SHGC low-e coatings, SHGC = 0.71, VT = 0.89, Emissivity = 0.04.

further increase visible transmittance while maintaining large IR reflection. Several previous studies have focused on anti-reflection films and wide bandgap semiconductors for developing the low-SHGC low-e coatings [40–43]. The anti-reflective layer is structurally tailored to these optical properties with patterned and porous structures via nanoimprint lithography or gradient refractive index [44,45]. The anti-reflective coating may not be particularly aimed at improved thermal performances, but the increased visible transmittance has strong potential to save overall energy by reducing cooling loads associated with the electrical lights [46].

It is worth noting that the spectra of the high-SHGC low-e coating (e.g. single silver unit, Fig. 3c) are quite different from those of the idealized (Type B, Fig. 3a), especially in the solar infrared region. It has been a great challenge to achieve coincident high solar-infrared transmittance and low emissivity in longwave radiation via the spectrally selective thin films. Fig. 4b shows 50% solar-infrared reflection to outdoor, which is far from the desired property of a perfect window. Destructive optical interference is a possible approach to increase solar-infrared transmission by adding dielectric or oxide layers with optimized thicknesses and refractive indices. However, in most of the weather conditions, strong solar-infrared transmittance may not be necessary from the practical standpoint, as cooling loads in summer, due to high IR transmittance, may offset the benefits in winter.

2.3. Absorption-based nanoparticle systems for spectral selectivity

A narrow waveband absorption in solar infrared, especially in the near-infrared (NIR) region (750–1300 nm) counting for 40% solar energy, has been studied as an alternative solar heat blocking mechanism in recent years [47–49]. Intrinsic absorptive properties of materials, such as tinting materials, pigments, and dyes, have been utilized in windows in order to absorb NIR. However, these material systems are known to pose negative effects on visible transmittance, instability, and haze conditions. In recent years, absorption-based nanoparticle-composites have been developed for the spectrally selective films. The absorption-based spectral selectivity thin films have been realized via special electronic properties of the nanoparticles, for instance, the localized surface plasmon resonance (LSPR). Several types of materials are known to absorb infrared and suitable for glazing applications. These include gold, ITO, AZO, antimony-doped tin oxide (ATO), lanthanum hexaboride (LaB_6), and rare-earth hexaborides (GdB_6) [50–54]. Among these, two candidates – ITO and LaB_6 have been extensively studied for glazing applications [51,54–60]. The ITO and LaB_6 nanoparticles are characterized with high transparency and absorption wavebands in particular infrared regions. The research effort has been focused on manipulating the absorptions into the desired regions. Schelm et al. incorporated both spherical LaB_6 and ITO nanoparticles into Poly(vinylbutyral) (PVB) and obtained strong absorptions at 900 nm and 2350 nm, respectively [54]. Yuan et al. reported the correlation between the particle size of LaB_6 in polymer and absorption level in the region of 600–1380 nm [60]. Adachi et al. found redshift and broadening of the LSPR peak in the disc-like LaB_6 nanopartcles [59]. In addition, these experimental works show considerable compositional effects on the infrared absorptions of the LaB_6 and ITO nanoparticles when dispersed in the PVB matrices. For instance, 0.3 wt% of LaB_6 plus 4 wt% of ITO doped in PVB matrix resulted in transmittance of 72.4% in visible (615 nm) and 55% in infrared (1000–2,250 nm) regions[58]. The optical properties can be further optimized through control of the particle size, shape, orientation, distribution, concentration, and composition for high-quality glazing

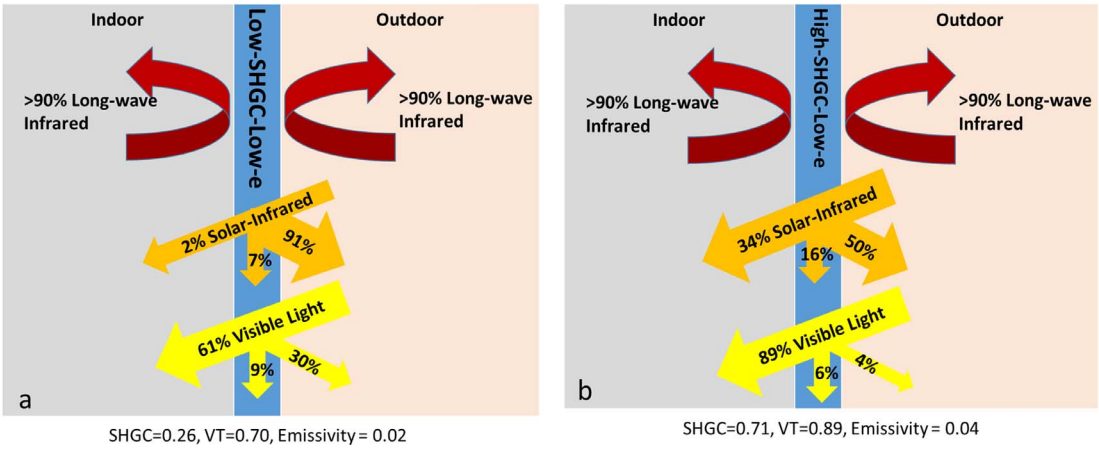

Fig. 4. (a) Typical optical properties of spectrally selective thin films with low SHGC, designed for hot weather or summer season. (b) Typical optical properties of spectrally selective thin films with high SHGC designed for cold weather or winter season.

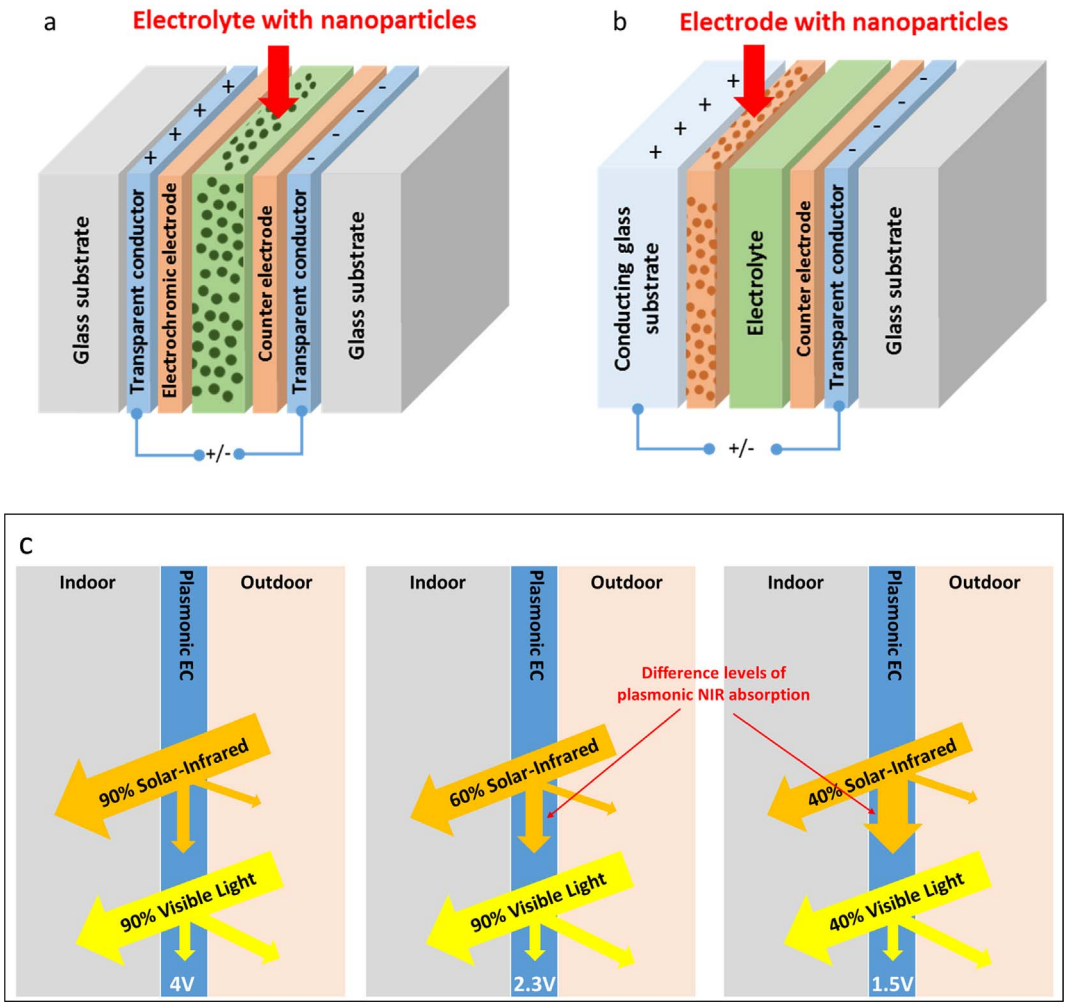

Fig. 5. (a) Structure of nanocomposite electrolyte with nanoparticles; (b) ITO nanocrystal–NbO_x film (deposited ion a conducting glass substrate) as the working electrode in an EC structure, and (c) three schematic status of the EC windows under 4 V, 2.3 V, and 1.5 V.

applications.

Thin films incorporating various nanoparticles may isolate visible and infrared radiations from solar spectrum. However, independent multispectral band modulations are still difficult for the visible or infrared radiations. The so-called electrochromic (EC) materials have been developed to address this critical issue in the past several decades. A new approach based on plasmonic electrochromism has recently been proposed and demonstrated by Milliron et al. [61,62] One of the unique features of EC materials is the ability to selectively control NIR absorption via modulated LSPR. Fig. 5 schematically illustrates this concept with two types of nanostructure designs of the EC thin films. As shown in Fig. 5a, the nanocomposite electrolyte consists of polymer hosts and transparent conducting nanoparticles such as ITO, AZO, and LaB_6 [63]. Under different electrical potentials, the LSPR absorption level is altered by controlling the electrochemical changes and in turn their electron density. This alteration enables modulation of solar-infrared absorptions with minor effects on the visible region. In Fig. 5b, development of the electrode based on depositions of ITO nanocrystals on niobium oxide (NbO_x) glass presents another viable approach [62,64]. Both ITO nanocrystals and NbO_x glass matrix exhibit distinctly different spectral electrochromic responses, therefore each may independently yield modulation in the NIR (ITO nanocrystals) and visible regions (NbO_x) [62]. Fig. 5c shows three schematic status of the EC windows under varied voltages. As shown in this figure, high transmission is achieved for visible light and most of NIR radiation under 4 V, preferably for the winter season. Large NIR absorptions with slightly reduced visible light is obtained under 2.3 V. At 1.5 V, transmittance is reduced for both NIR and visible light [62]. In this way, one may design unique nano and electronic structures for tunable absorptions in different wavelengths.

As aforementioned, all previous studies focus on optimization of optical behaviors via spectral-selective features of media, associated with either their intrinsic or extrinsic materials properties. In other works, most of the effort has all concentrated on manipulation of optical properties (absorption/reflection in particular wavelength range) for optimum energy efficiency. However, spectral selectivity is often hindered by the intrinsic and extrinsic materials properties that are not easily manipulated via chemical and materials means. Quite often additional physical fields (such as electrical potential in spectral electrochromic) are required to fine-tune the optical properties. These obstacles often introduce additional complications in materials design, synthesis, and large-scale processing, which makes the engineering aspect not economical. Therefore, in further optimization of energy efficiency, new approaches, other than optical spectral selection, must be sought via different physical fields such as thermally-activated nanostructures that not only effective in thermal insulation, but also easily mass-produced with economic advantages.

Photothermal effect, although a well-known phenomenon especially in metallic materials, has been recently utilized, through some novel materials designs, for developing energy efficient architectural materials. A novel concept has been recently formulated in the design of single-pane windows with significantly enhanced thermal insulation

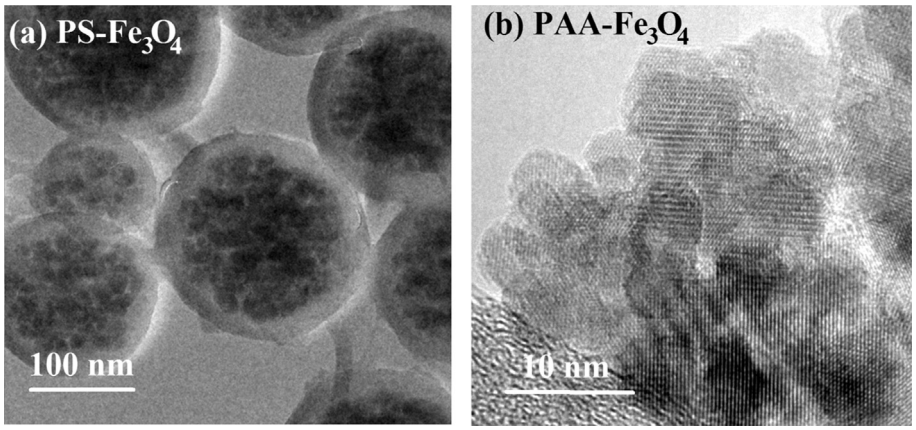

Fig. 6. (a) TEM image of PS/Fe_3O_4 microspheres showing the polystyrene spheres entrapping multiple Fe_3O_4 nanoparticles, and (b) TEM image of PAA/Fe_3O_4 [65].

based on the photothermal effects of oxide nanoparticles, such as Fe_3O_4. The following sections will be devoted to the new design of nanostructures, their synthesis and physical properties, and potential applications in energy-efficient windows especially for the cold climate regions. It should be noted that saving building energy via the photothermal effect of nanostructures is a very new development with the first paper published in 2017 [65]. In particular, all previous photothermal studies have focused only on solutions and particles for medical applications. Investigation on photothermal thin films is also recent therefore with limited literature. Nonetheless, it points to a new direction in the development of optical energy materials with the high possibility of achieving the most energy-efficient materials.

3. Part II window designs based on the photothermal effect of nanomaterials

3.1. The concept of photothermal effect and opportunities in window applications

Recently, photothermal hyperthermia of nanoparticles via NIR irradiation has been developed for various applications including medical therapy [66–76]. The photothermal effects have been found in several nanoparticle systems, such as quantum dots, gold, graphene, and Fe_3O_4 [66,67,69,71,72,74–76]. These nanoparticles all exhibit strong NIR-induced photothermal effects effectively raising the solution temperature by greater than 30 °C. The previous studies show that, upon NIR-laser irradiation, the temperature of the Fe_3O_4 nanoparticle aqueous suspensions can increase, within short periods of time, from room temperature to 45 °C [69,72,74,76]. However, these photothermal studies were all based on NIR radiation (~800 nm). The photothermal effects of these nanoparticles via a much wider spectrum (350–750 nm) have not been rigorously investigated. In particular, the photothermal mechanism under solar light was not investigated for Fe_3O_4 until very recently.

The photothermal effect has been extensively studied for gold and graphene and attributed the energy conversion to LSPR [68,70,73]. A localized plasmon is the result of the confinement of a surface plasmon in a nanoparticle smaller than the wavelength of the incident light. A nanoparticle's response to the oscillating electric field can be described by the so-called dipole approximation of Mie theory [77]. The fluorescent quantum dots were also found to exhibit highly efficient photothermal effect [75]. Although the photothermal effects of these nanomaterials have been shown to be effective, they are quite costly making them not industrially viable especially for large surfaces and volumes. Furthermore, the operating mechanisms of heat conversion have not been well identified for some of the semiconducting systems. We have recently investigated the photothermal effect of the Fe_3O_4 nanoparticles and explained its mechanism based on the photoluminescence emission in both visible and NIR regions [74,76].

Spectrally selective thin films based on the plasmonic NIR absorption present a promising approach to achieve independent multispectral band modulations. However, regardless of the optical property, be it static or dynamic, these thin films regulate solar spectrum transmission mainly through the absorption rather than reflection. Consequently, glazing systems with these thin films necessitate the use of low-e coatings. In addition, the longwave radiation control still relies on low-e coatings in winter while blocking the external longwave heat in summer. The low-e coating can reflect about 50% solar-infrared radiation in the winter season, which is essentially “free” from the environment (Fig. 4b). There is, therefore, a high incentive to fully utilize this free energy via new window structure designs, especially for retrofitting the existing windows.

3.2. Synthesis and characterization of the Fe_3O_4 nanoparticles

We have recently shown that the Fe_3O_4 nanoparticles, in various forms, can generate sufficient heat when irradiated by NIR light (808 nm) [74,76]. By directing a low-power laser beam into a solution of weak concentration of magnetic Fe_3O_4 nanoparticles, the solution temperature rapidly reached above 42 °C. One of the unique nanostructures is the polystyrene (PS)/Fe_3O_4 composite. Nanoscale Fe_3O_4 nanoparticles (~5–10 nm) are embedded in the matrices of PS spheres that are synthesized by using modified emulsion/miniemulstion polymerization [74]. The Fe_3O_4 nanoparticles with an average particle size about 10 nm were synthesized and dispersed in situ in octane as a ferrofluid. The ferrofluid was then added to the aqueous solution with sodium dodecyl sulfate (SDS) to obtain miniemulstion after ultrasonication. Meanwhile miniemulstion was prepared from styrene monomer. The mixture was held at 80 °C for 20 h in order to obtained the Fe_3O_4/PS nanospheres (Fig. 6a). The poly(acrylic acid) (PAA) coated Fe_3O_4 nanoparticles was obtained by co-precipitation of iron chloride salts with ammonia, denoted as PAA-Fe_3O_4 [74]. Fig. 6a depicts multiple nuclei of Fe_3O_4 entrapped within a polystyrene matrix while Fig. 6b shows the image of PAA-coated Fe_3O_4. The particle diameters can be estimated in the focal plane if the nanoparticles are known to possess a generally spherical geometry. The nanoparticles that are not surface functionalized are denoted as Uncoated Fe_3O_4. Their morphologies are similar to those shown in Fig. 6b.

3.3. Photothermal effect measurements using near-infrared laser

The photothermal measurement apparatus is schematically shown in Fig. 7. The sample is injected into one well of a 48-well microplate. The microplate is placed on an electric hot plate, which is in an incubator, to provide a 37 °C environmental temperature. A 785 nm laser with controllable power supply (0–1 A, 6 V) is used as the light source, as shown in Fig. 7. The shape and size of the light spot is set to exactly cover the sample well. The sample surface temperature is recorded by

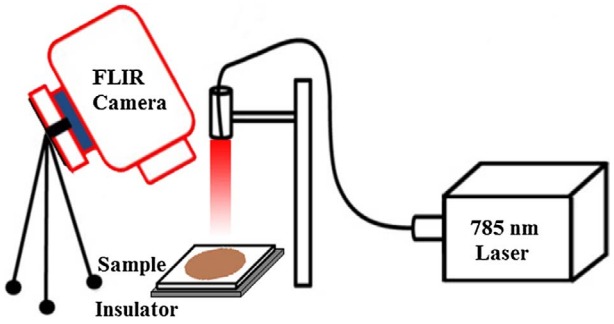

Fig. 7. Apparatus for photothermal experiment.

an infrared camera (FLIR-T640). The well bottom area is 0.95 cm^2, and an optical power meter is used to measure the laser power on the sample surface. A standard power meter can be used to determine the relation between the applied current and the optical power output. A linear function can also be fit to the data to allow calculation of the laser power and consequent intensity over an applied area. For a given nanoparticle concentration, laser intensity and wavelength, a heating and cooling curve can be generated. The infrared camera is oriented to monitor the temperature of the nanoparticle solutions. For determination of the heating curve, temperatures are normally recorded every minute for the first 8 min and every two minutes for the next 12 min. The cooling curve is obtained by recording the temperature at 30 s, 1 min, and every following minute for the next 7 min after removal of the laser.

Fig. 8 shows the heating curves for 150 μl of PAA-Fe_3O_4 [74]. The photothermal effect was observed by application of 38.5 kW/m^2, 785 nm NIR laser for 15 min. Temperature was measured through IR thermal imaging by a FLIR-T640. Sapareto and Dewey showed that concentration of 0.2 mg/ml was the minimum expected for inducing significant photothermal effect at an intensity of 38.5 kW/m^2 and an application time of 15 min [78]. As can be seen in Fig. 8, there is an obvious concentration dependence of the photothermal effect. At 1 mg/ml, the temperature rapidly increases to 60 C, within first 5 min, then saturates afterwards. It is also observed in this figure that the nanoparticles exhibit considerable photothermal effects even at low concentrations such as 0.1 mg/ml, raising temperature above 40 °C.

3.4. Photothermal effect measurements using solar light

Zhao et al. recently investigated the photothermal effects of Fe_3O_4 nanoparticles and thin films in a much wider spectrum [65]. In their experiments, a white light was applied using a solar simulator for generating the photothermal heat in Fe_3O_4 nanoparticle suspensions and thin films. In the "sample-in-well" experiment, 0.15 mL solution with different Fe_3O_4 concentrations (0.25, 0.5, 1.0 mg/mL) was added

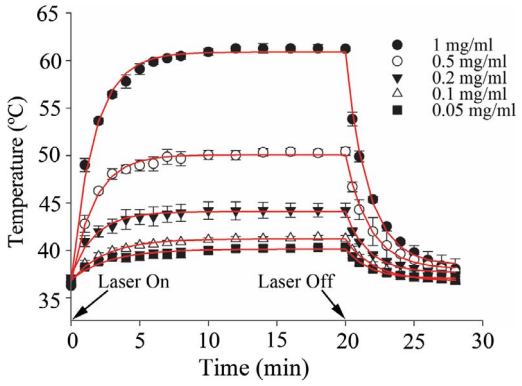

Fig. 8. PAA-Fe_3O_4 heating curves [74].

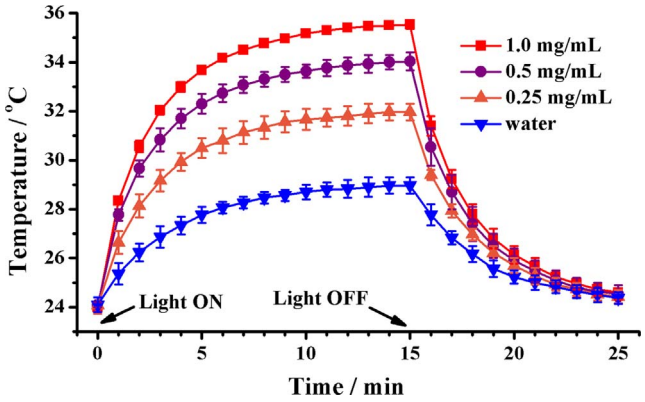

Fig. 9. Temperature *vs.* time curves for different concentrations of PAA-Fe_3O_4 solutions under white-light irradiation. Intensity of the illuminated light: 0.1 W/cm^2 [65].

into a 48-well plate [65]. For the "sample-on-glass" experiments, a solution with 0.1 mg Fe_3O_4 nanoparticles was coated on a 25 mm × 25 mm glass slide by drop casting in order to develop a thin film [65]. Both the liquid and thin film samples were irradiated by a white light from a solar simulator. The power density on the samples from both light sources is 0.1 W/cm^2, which is about the sun radiation density on the Earth. The sample temperature was measured by the thermal imaging camera. Light was turned on for 15 min, but the thermal imaging camera continued to record the temperature after the light was turned off. All preliminary experiments started from room temperature.

Fig. 9 shows the heating curves of PAA-Fe_3O_4 solution at various concentrations (0.25, 0.5 and 1.0) mg mL^{-1}. A solar simulator was used as the light source at the light intensity of 0.1 W/cm^2, which provides approximately the radiation density similar to the surface of Earth from sun. As can be seen in this figure, as expected, the photothermal effect has a clear concentration dependence. At 0.1 W/cm^2, the 1.0 mg mL^{-1} sample results in a temperature increase of 11 °C (from 24 °C to 35 °C) within 15 min. Even at 0.25 mg mL^{-1}, the temperature of the solution could reach 32 °C, indicating a strong photothermal effect. Upon turning off the light source, as shown in Fig. 9, all samples exhibit approximately the same cooling rates indicating similar heat losses to the surroundings [65].

The heating curves of the same PAA-Fe_3O_4 solutions are shown in Fig. 10. These curves were obtained by using a 785 nm NIR laser irradiation with light intensity of 0.1 W/cm^2. The NIR laser generates, as can be seen in this figure, much less heating compared to the white-light irradiation at1.0 mg mL^{-1}. The temperature only increases slightly from ~23.5 °C to 27 °C, resulting a gain of 3.5 °C within 15 min.

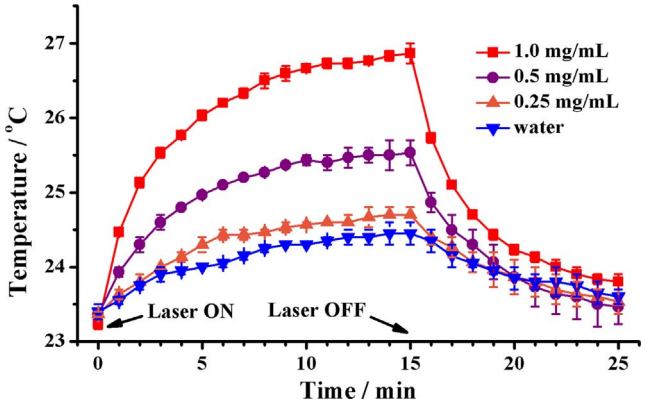

Fig. 10. Temperature *vs.* time curve for different concentrations of PAA-Fe_3O_4 solutions under 785 nm laser. Intensity: 0.1 W/cm^2. Note the same samples are used in obtaining heating curves shown in Fig. 9 [65].

Expectedly, even weaker heating is observed at 0.25 mg mL^{-1} for an insignificant temperature increase. These results clearly show different photon absorptions and energy conversions between NIR and white light irradiations. It is evident that white light produces much greater photothermal effect and heating efficiency.

3.5. Coating of polymer thin films on glass

For energy efficient window applications, spin coating was preferred and used to deposit thin films on the glass substrate in an experiment recently reported by Zhao et al. [65]. Spin coating is economically viable and technically straightforward, therefore commonly used to deposit uniform thin films to flat substrates [79]. The solution containing Fe_3O_4 nanoparticles of various concentrations is applied on the center of the substrate, that is spinning at a controlled low speed. In the experiments reported by Zhao et al., the substrate was kept still for obtaining a film of certain thickness. Different polymer materials may be selected for thin film coatings on glass that exhibit most efficient heating but high transparency. Note that the balance between the photothermal efficiency and transparency has to be well controlled for the optimum optical properties. Ideally, the thin film coating should exhibit the highest transparency while exerting the strongest photothermal heating. The balance is difficult as well-diluted solution coating may have a high transparency but attenuated photothermal effect. Further, the window should also have good spectral selectivity, as described above that most of NIR should be well absorbed in the winter for energy saving. It is therefore important to develop nanomaterials with both strong photothermal and spectral selective properties for energy efficient window applications.

By carefully selecting the type and thickness of the polymer layers, one can deposit Fe_3O_4 nanoparticles on a single pane using the spin coating method, as it is the most economic approach compared to the vapor deposition for building structures.

3.6. Photonic properties of the Fe_3O_4 nanoparticles

As briefly described above, the photothermal effect has been attributed to the LSPR of the nanoparticles under light irradiation. The LSPR effect has been previously demonstrated for both noble metals and conducting metal oxides (CMOs) [68,70,73]. Even for low charge carrier densities of CMOs ($n \approx 10^{21}$ electrons/cm^3), compared to that of typical noble metals ($n \approx 10^{23}$ electrons/cm^3), LSPR effect can arise from limited conductivity. LSPR behavior is associated with conducting electrons of any materials with considerable charge carrier densities oscillating in response to electromagnetic waves. According to Drude free electron model [80]:

$$\omega_p = (ne^2/\mu\,\varepsilon_o)^{1/2} \quad (1)$$

where ω_p is the plasma frequency, μ is the effective mass, n is the charge carrier density, e is the electron charge, and ε_o is the permittivity of vacuum. Based on this equation, for typical conducting metal oxide, the plasma frequency is on the order of 1 eV in the NIR region. For gold nanoparticles, there have been studied that show considerable absorptions in the NIR range, providing the energy conversion for photothermal effect [81].

The UV–VIS–NIR absorption spectra of the Fe_3O_4 nanoparticles were previously obtained from wavelength range between 300 nm and 950 nm [82]. The absorption co-efficient (α) as a function of photon energy (E) is shown in Fig. 11 for different types of nanoparticles indicated [82]. α obeys a relationship [83]:

$$\alpha = \alpha_0 \exp\left[\frac{\sigma(E-E_{0)}}{k_B T}\right] \quad (2)$$

where α_0 is the absorption coefficient, E is the incident energy, E_o is the onset of absorption, and $E_u = k_B T/\sigma$ is the Urbach energy, where σ is

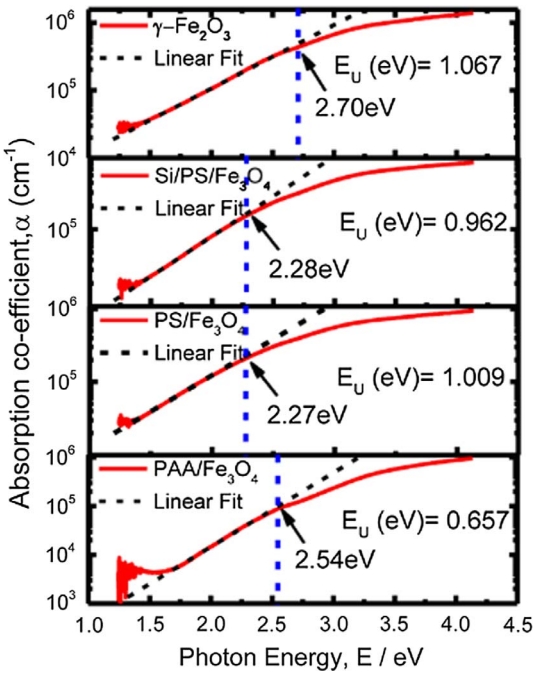

Fig. 11. UV–VIS–NIR absorbance spectra of various Fe-O nanoparticles indicated [82].

the steepness parameter and k_B is the Boltzmann constant. Urbach energy is a parameter related to the crystal defect density associated with impurities and disorder. Both α_o and E_o in Eq. (2) are material-dependent constants, and observed for many ionic crystals, degenerately doped crystalline, and amorphous semiconductors [83]. Some of the defects are thermally activated such as point defects in oxides, leading to an Urbach exponential absorption tail. In Fig. 11, one can see that the Urbach energy is obtained from the linear portion of the log α vs. photon energy curve for various Fe_3O_4 nanoparticles indicated. These include the PAA-coated Fe_3O_4 nanoparticles (PAA/Fe_3O_4) and Fe_3O_4 nanoparticles embedded in polystyrene nanospheres (PS/Fe_3O_4). Si/PS/Fe_3O_4 denotes the silica-surface-functionalized PS/Fe_3O_4. The Urbach Energy values were determined to be 0.572 eV, and 0.418 eV respectively for the Uncoated Fe_3O_4 and PAA-Fe_3O_4. The lower Urbach Energy (0.418 eV) is an indication of effective modification of Fe_3O_4 nanoparticles by PAA resulting in reduced surface defects [82]. By plotting $(E\alpha)^2$ as a function of photon energy, the direct band gap can also be estimated from extrapolation of the linear portion of the curve to the x axis which gives the value of the direct band gap. The extrapolation shows the energy difference (~3.1 eV) between O(2p) and (e_g) of the octahedral site [82,83].

The previous experimental results show that Fe_3O_4 nanoparticles exhibit continuous decrease in photon absorption up to the NIR region (i.e. no obvious strong absorption in NIR), while strong absorptions in the visible region (~530 nm) have been well observed for gold nanoparticles, responsible for strong photothermal effect [72,84,85]. According to the discussion on the ideal window, it is preferred to have strong absorption in the NIR region for that to be converted to the photothermal energy in winter. To deal with this issue, a Fe_3O_4–Ag hybrid may offer the required optical properties [85]. Bankole and Nyokong developed a Fe_3O_4/Ag (Fe/Ag) core–shell structure that exhibits considerable photon absorption near 690 nm [85]. They attribute photon absorptions to the LSPR effect for the Fe_3O_4–Ag hybrid and explained the red shift by the depleted electron density at the Fe_3O_4–Ag interfaces. However, the mechanism of NIR absorption is still not well identified for the Fe_3O_4/Ag (Fe/Ag) core–shell structure. Nonetheless, the NIR absorption observed in the Fe_3O_4–Ag composite nanoparticles present some potential for making the energy efficient energy windows.

Sadat et al. observed photoluminescence (PL) in both visible and

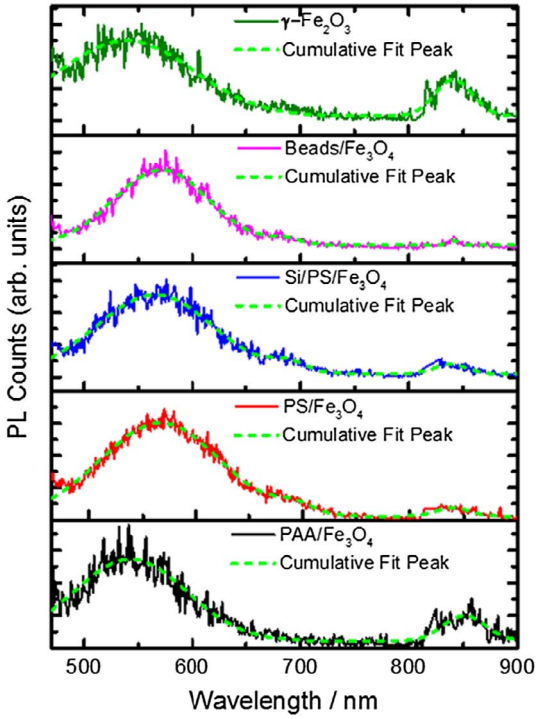

Fig. 12. Photoluminescence spectra of various Fe-O nanoparticles indicated [82].

NIR regions for Fe_3O_4 nanoparticles in various forms [82]. Fig. 12 shows the PL spectra of the PAA/Fe_3O_4, PS/Fe_3O_4 and Si/PS/Fe_3O_4 measured at 10 mg/mL with a solid state laser of 4.5 mW and excitation wavelength 407 nm (3.04 eV). They found the most intensive peak at ~540 nm (2.296 eV) for PAA/Fe_3O_4 while those for the PS/Fe_3O_4 and Si/PS/Fe_3O_4 are at ~565 nm (2.194 eV). The emissions near 540 nm and 565 nm were respectively assigned to the energy gap of crystal field splitting (2.2 eV) of octahedral site and the electron transitions between the defect sites [82].

Zhao et al. also found the PL emissions from the PAA-functionalized Fe_3O_4 nanoparticles (Fig. 13). In particular, they observed a clear NIR peak at 674 nm (1.84 eV). As can be seen in Fig. 13, the peak at 550 nm (2.10 eV) in the visible region is much broader. This is consistent with the experimental data that the photothermal effect is more pronounced when irradiated by the white light compared to 785 nm laser, as the former contributes to photon absorption in a wider frequency range. The PL peak at NIR was suggested by Sadat et al. to correspond to the

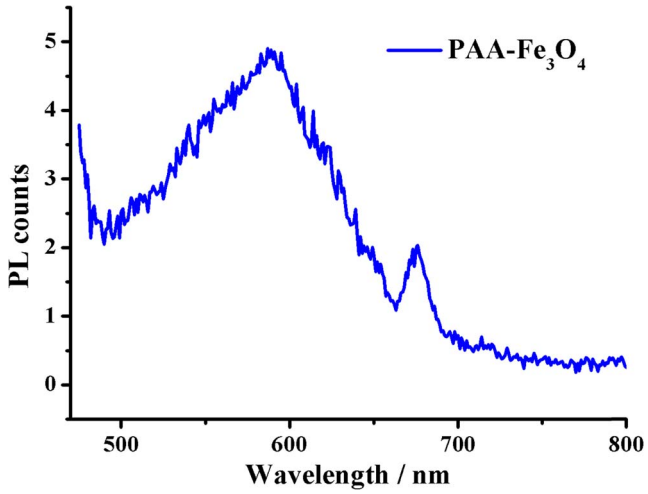

Fig. 13. Photoluminescence spectrum of PAA-coated Fe_3O_4 nanoparticles [65].

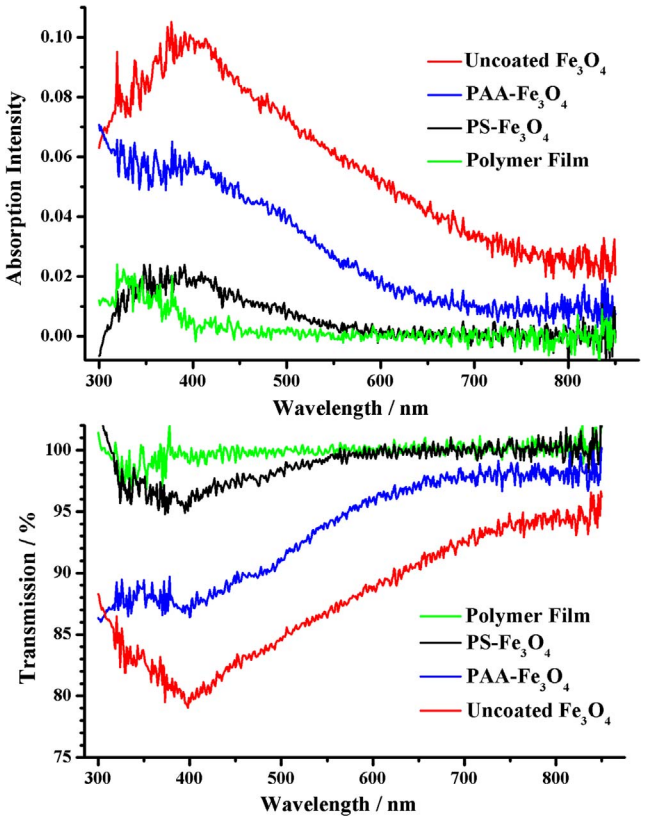

Fig. 14. (a) Absorption intensity *vs.* wavelength for thin samples containing various Fe_3O_4 nanoparticles indicated; (b) Transmission *vs.* wavelength for thin samples containing various Fe_3O_4 nanoparticles indicated [65].

recombination of trapped electrons from the octahedral site to O(*2p*) on the tetrahedral site[82].

For window applications, as mentioned above, transparency, upon nanoparticle coatings, is important while maintaining the optimum optical properties such as considerable absorption in NIR, strong photothermal effect, and high photon transmission in the visible range. Fig. 14 shows the absorption and transmission for various thin film coatings on the glass substrates. As can be seen in this figure, the highest absorption, thus lowest transmission, is observed for the thin film containing the uncoated Fe_3O_4 nanoparticales. A peak near 400 nm is also evident, rendering this film rather dark under visible light. The situation improves when the nanoparticles are coated with poly acrylic acid (PAA), as shown in Fig. 14. Much higher transmission is achieved when the Fe_3O_4 nanoparticles are embedded in the polystyrene nanospheres, however with compromised photothermal effect. Fig. 15 shows the heating curves of thin films containing Fe_3O_4 nanoparticles in various forms. Consistent with Fig. 14, the film with the uncoated-Fe_3O_4 nanoparticles exhibit the strongest photon absorption and highest photothermal effect (Fig. 16). The film with PAA-coated Fe_3O_4 nanoparticles shows reduced visible absorption, and correspondingly lower photothermal effect. The substrate with the PS/Fe_3O_4 coating is quite transparent, but suffers from the significantly weakened heating ability. It is thus important to consider these optical and photothermal properties in thin film design and nanoparticle development so that both transparency and photothermal heating efficiency are enhanced simultaneously.

Sadat et al. calculated the extinction (Q_{ext}), absorption (Q_{abs}), and scattering (Q_{sca}) efficiencies using the following equations [82,86]:

$$Q_{ext} = \frac{2}{x^2}\sum_{n=1}^{\infty}(2n+1)\mathrm{Re}[a_n + b_n] \quad (3)$$

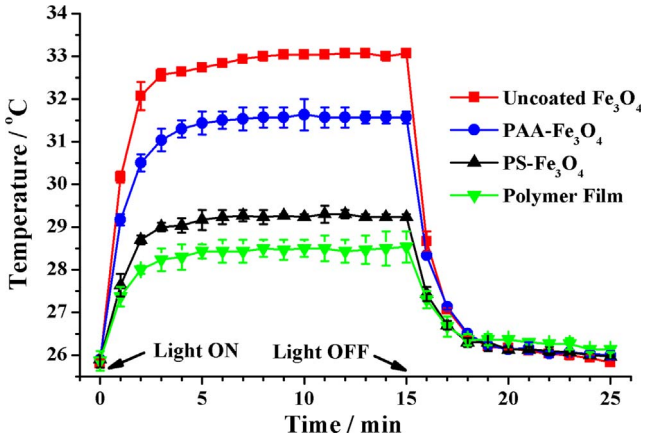

Fig. 15. Temperature *vs.* time for the thin film samples containing various Fe_3O_4 nanoparticles indicated. There is 3 mg Fe_3O_4 per slide. Heating power: 0.1 W/cm^2 [65].

$$Q_{sca} = \frac{2}{x^2}\sum_{n=1}^{\infty}(2n+1)[|a_n|^2 + |b_n|^2] \tag{4}$$

$$Q_{abs} = Q_{ext} - Q_{abs} \tag{5}$$

where $x = \frac{2\pi n_{med} a}{\lambda_0}$ is the size parameter; a is the mean radius of the particles, n_{med} is the refractive index of the media, and λ_o is the vacuum wavelength. Both a_n and b_n are the coefficients. The Q_{ext}, Q_{abs} and Q_{sca} values were calculated using the code of "Mie-Plot" by Philip Laven and plotted as a function of wavelength as shown in Fig. 16 [87]. Sadat et al. pointed out that the extinction efficiency of PAA-Fe_3O_4 is mainly dominated by absorption (see curves of Q_{ext} and Q_{abs} in Fig. 16a) while considerable scattering is evident in PS/Fe_3O_4 (see curve of Q_{sca} in Fig. 16b). This difference may explain the much lessened photothermal effect in the latter [82].

3.7. Calculation of the photothermal conversion efficiency

For the photo energy transferred to heat, the conversion efficiency can be calculated. Han et al. calculated the photothermal conversion efficiency, η, of silica-functionalized Fe_3O_4 composites using formulations developed by Roper et al. The photothermal conversion efficiency η can be expressed as [88,89]:

$$\eta = \frac{hS(T_{Max} - T_{Surr}) - Q_s}{I(1-10^{-A_{808}})} \tag{6}$$

where the proportionality constant h (mW/(m^2 °C) is the heat transfer coefficient; S (m^2) is the surface area of the container; T_{Max} (°C) is the system maximum temperature; T_{Surr} (°C) is the ambient surrounding temperature; QS (mW) is the energy input by the sample cuvette and the solution; and I is the incident light power.

The value of hS is obtained by the following equation [88]:

$$hS = \frac{\sum_i m_i C_{P,i}}{\tau_s} \tag{7}$$

where m_i and $C_{P,i}$ are respectively the mass and heat capacity of the sample including nanoparticle suspension and sample cell. τ_s (s) is the sample system time constant which is given by [89]:

$$\tau_s = -\frac{t}{\ln\theta} \tag{8}$$

where θ is defined as the ratio of $(T - T_{surr})$ to $(T_{Max} - T_{surr})$, and T (°C) is the solution temperature. ɵ can be expressed as [88,89]:

$$\theta = \frac{T - T_{Surr}}{T_{Max} - T_{Surr}} \tag{9}$$

where $(T_{Max} - T_{Surr}) = \Delta T$ and is experimentally determined. With all experimental conditions and parameters provided in the study by Han et al, they calculated the η value of 31.9% for the nanoparticle solution [89]. The general formulations and calculations will have to be established for the η values of thin films on the glass substrates with given materials properties and dimensions. The photothermal conversion efficiency will also have to be optimized through both nanomaterials development and multilayer thin film structure designs.

4. Discussion

As we discussed in Parts I and II, spectrally selective thin films and photothermal thin films focused on different fundamental physical mechanisms related to solar light, which is mainly about optical and thermal, respectively. Utilizing both spectral selective features and photothermal effects of nano structured thin films may achieve independent multispectral band modulations while fully utilizing "free" solar energy which is normally reflected by low-e coating and converting it to thermal energy in winter. Fig. 17 shows the schematic diagram on a new window design based on the phototheraml effect and spectral selectivity. In this proposed schematic design, we selected Fe_3O_4 nanoparticles as the photothermal medium. One of the most investigated nanomaterials is Fe_3O_4 for its pronounced photothermal effect in biomedical applications [66–75]. The Fe_3O_4 nanoparticles can be dispersed in various solutions upon surface functionalization. Deposition of thin film coatings on windowpanes is therefore possible to improve the overall winter center-of-glass U-factor of windows with strong Fe_3O_4 photothermal effect. The working mechanism is as follows.

The adjacent low-e coating layer is heated up by conductive heat transfer from the Fe_3O_4 layer. The convective heat transfer at the interior window surface plays an important role in the overall window

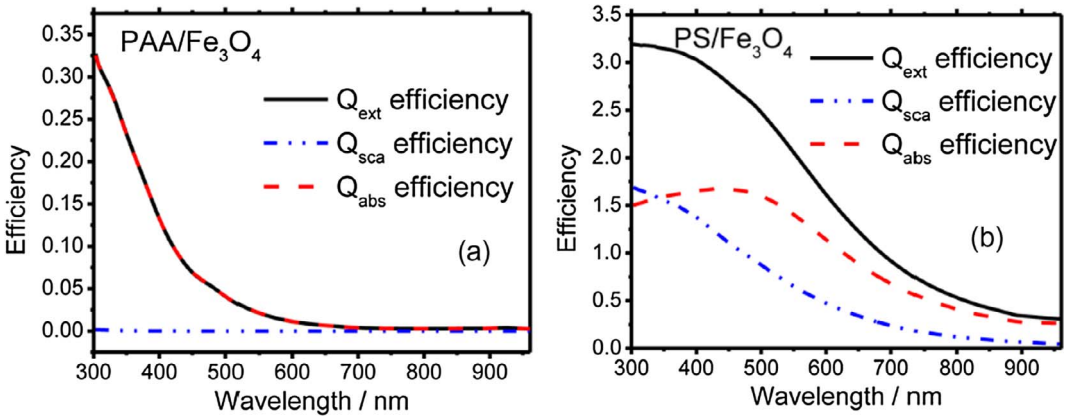

Fig. 16. Extinction (Q_{ext}), absorption (Q_{abs}), scattering (Q_{sca}) efficiencies as a function of wavelength for PAA/Fe_3O_4 (a) and PS/Fe_3O_4 (b), respectively [82].

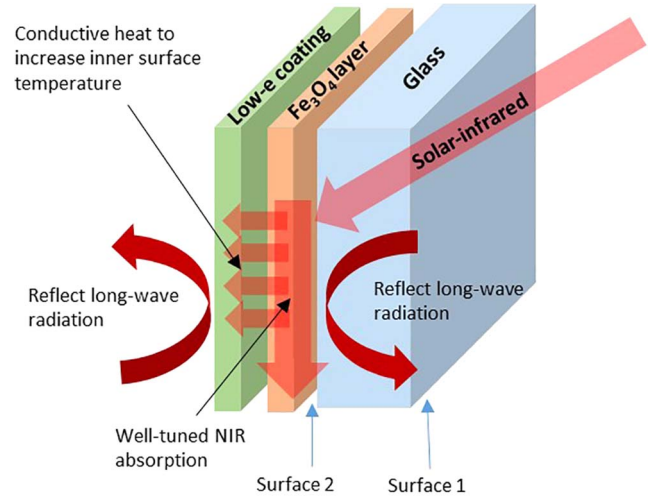

Fig. 17. A typical glazing structure with absorption-based spectrally selective thin films.

thermal performance in the winter season. This is a particularly important architectural feature that the forced airflows via air vents are generally located under windows in a building. The solar-induced photothermal heating on the inner surface of windowpane can then be used to effectively reduce the temperature difference ΔT between the warm room interior and the window glass interior surface in the winter season, therefore diminishing the convective heat loss significantly. Meanwhile, the low-e coating still serves as a longwave radiation reflector to keep indoor warm conditions. Unlike the conventional "heat-absorbing" tinted glasses with low visible transmittances, the nano-composite coating shown in Fig. 17 absorbs insignificant visible light, but the narrow waveband near-infrared radiation. In this way, there will be little or no change in visual appearance and transmittance.

Regarding possible summer overheat situation, one can design a window external layer (Surface 1 in Fig. 17) based on optical constructive interference on a selective waveband according to the solar energy incident angles, while still allowing maximum transmission in winter. Similarly, angular selective films with nano structural characteristics have been developed to reflect, divert, and scatter light into designated directions for angular dependent transmittance [90,91]. Expected absorption intensity curves for the combined effects from the photothermal layer and the external summer heat control layer are shown in Fig. 18. In winter, the photothermal layer selectively absorbs the incident solar-infrared and the low-e coating layer reflects NIR radiation, focusing the thermal energy to heat up the inner window surface for reduction of convective heat transfer. In summer, upon mitigation effect by the external interference layer or angular selective layer, the absorption intensity of the photothermal layer is reduced to a lower level compared with that in winter, rendering a minor temperature increase.

Regarding the effects by different orientations of windows on buildings, this window structure design could still operate as what we designed to convert the absorbed NIR solar energy to thermal energy but more thermal energy will be obtained during the early morning for east façade and the late afternoon for west façade due to the strong incident solar light at the low solar altitude. Detailed data collections on solar irradiance and its NIR potion for different vertical orientations should be conducted in future works for this analysis.

In order to understand the improvements of window thermal insulation, we calculated U-Factor using hypothesized photothermal effects on single-pane windows. In the United States, National Fenestration Rating Council (NFRC) implements a national rating system for energy performance of fenestration products, and NFRC has standardized the environmental conditions for U-factor calculations (interior air temperature: 21.1 C, exterior air temperature: −17.8 C, wind speed: 12.3 km/h) [77]. U can be expressed as [92]:

$$U = \frac{1}{\frac{1}{8.07 \times v^{0.605}} + \frac{1}{1.46 \times \left(\frac{T_3 - T_1}{L}\right)^{0.25} + \sigma e \left(\frac{(T_3 + 273.16)^4 - (T_1 + 273.16)^4}{T_3 - T_1}\right)} \times \left(\frac{T_3 - T_2}{T_3 - T_1}\right)} \tag{10}$$

where L is the total height of a window, σ the Stefan–Boltzmann constant ($5.67 \times 10^{-8}\,W/m^2K^4$), e is emissivity, T_1, T_2, and T_3 are the window's inner surface temperature, window's outer surface temperature, and indoor air temperature, respectively.

Eq. (10) can be used to analyze the possible impacts of the inside surface temperature T_1 (which can be controlled by the photothermal effect) on the center-of-glass U-factor. In this estimation, we hypothesized two groups of glazing systems: high emissivity ($e = 0.87$) and low emissivity ($e = 0.03$). In addition, each group has three different baseline insulation referring to the three possible outside surface temperature T_2. Regarding the group with the high emissivity ($e = 0.87$), increasing temperature T_1 can dramatically lower U-factor for all three types of glazing systems. The decrease is ~28–68% depending on the increase of the temperature T_1 for the three glazing systems. For low emissivity ($e = 0.03$), the reduction percentage is around ~21–65% for the three glazing systems.

Under the NFRC standards, based on Eq. (10), the possible impacts

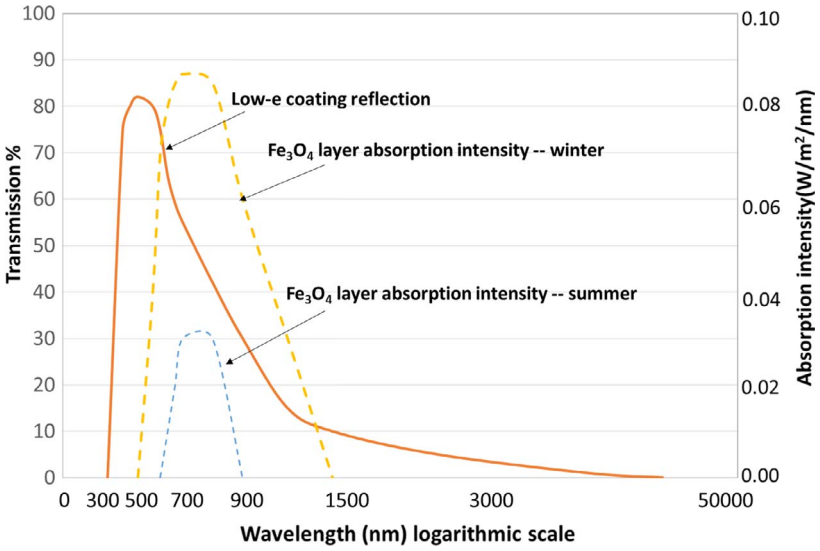

Fig. 18. Expected absorption intensity curves of the photothermal layer in winter and summer as a function of wavelength. The reduction is due to the mitigation effect by the interference layer or angular selective layer on window surface 1 (Fig. 17).

of ΔT on the center-of-glass U-factor of Fe_3O_4 thin films. In their photothermal experiments, they found the temperature of the Fe_3O_4 thin film typically increased approximately 5 °C after white light irradiation. Assuming a similar ΔT under the experimental conditions, the center-of-glass U-factor was found, according to their calculations, reduced to 0.08–0.15 W/m^2 K. The U-factors in this range would correspond to an energy saving of 85–159 KJ/m^2 in one-hour white light irradiation. This U-factor estimation demonstrates the potentials of the photothermal effect under white light in the design and application of the energy efficient windows.

Based upon a DOE report, the stock of sing-pane window is declining fairly slowly. About 30% of residential buildings in cold U.S. climates uses the single-pane windows [1]. The concept depicted in Fig. 17 paves a new way for the most efficient window thermal insulation without relying on sandwiched window structures of two or three panes for heating-dominated locations. Furthermore, the Fe_3O_4-nanoparticle-containing polymer films can be applied using various coating methods, representing an ideal candidate for wide-scale-energy-efficient window retrofits with low balance-of-system costs. However, to achieve the goals illustrated in Fig. 18, the photothermal effect has to be studied in terms of various thin film parameters such as concentration, thickness, and heating efficiency. The operating physical mechanisms governing the photonic heat conversion will also have to be identified. Based on the photonic property study, the overall window thermal transfer mechanisms under all conditions can be investigated using both computational and experimental models. Upon optimization of photothermal efficiency of nanoparticles, prototypical single-pane models may be built for proof of concept.

5. Conclusions

This review concludes that it is possible to achieve a significant reduction in building energy consumption via design of novel nanostructures for window applications. Two conventional approaches are introduced for achieving the so-called “perfect window,” categorically, structural and spectral. The former deals with conventional glazing using sandwiched structures with the transparent insulation materials and/or air gas layers. The latter is concerned with spectral selectivity of windows in different wavelengths (from visible to NIR). Low-e coatings are spectrally selective control films that fall into this category. There is an abundant solar energy, 50% of which is directly reflected when it encounters the high-SHGC low-e coatings for cold climates, but can be otherwise utilized via the photothermal effect. Based on the perfect window concept, unidirectional NIR radiation is needed, yet difficult to achieve with the static thin films. In contrast, dynamic thin films, including electrochromic, thermochromic, electrophoretic, and suspended-particles, are capable of responding to external stimuli by changing their optical and physical properties, therefore highly promising for independent modulation in the visible and NIR regions.

Conducting nanoparticles exhibit strong plasmon absorptions in NIR region, while semiconducting oxides are less investigated for their photothermal effects. Recent studies on the Fe_3O_4 nanoparticles show photo-fluorescence in both visible and NIR regions, suggesting a possible mechanism for the photothermal effects that have been experimentally well observed. Although the photothermal effects of nanoparticles have previously and primarily used for cancer treatment, new studies suggest high possibilities for applications in energy efficient window structures. The traditional thermal insulation is accomplished via a gaseous gap between the double panes. The performance of the traditional double pane is therefore solely dependent on the thermal insulation properties of medium. It has been established in a recent study that the center-of-glass U-factor can be effectively reduced by photothermal heating of the window interior surface. By a straightforward coating method, a thin film containing Fe_3O_4 nanoparticles can be applied on the glass substrate. Upon simulated solar light irradiation, the surface temperature can be considerably increased resulting in reduced convective heat loss in winter. This is a fundamentally different approach in reducing window heat loss in winter via the photothermal effect of nanomaterials. This approach lifts some of the major obstacles to building energy savings and paves a new path for novel window designs.

The advantages of the photothermal thin films are several-folds: (1) no insulating medium is needed as in the traditional double-pane structure, (2) the Fe_3O_4 nanoparticles can be mass-produced with low cost, (3) the polymer coating containing Fe_3O_4 can also be easily applied using various coating methods, (4) ΔT between the warm room interior and the inner window glass surface temperature can be tuned by adjusting the nanoparticle concentration and film thickness, (6) the condensation resistance in glass corners and edges can be increased by directing magnetic Fe_3O_4 nanoparticles to the specific areas of glass, and (7) adhesive products built upon this approach can be applied in wide-scale energy-efficient window retrofits with low balance-of-system costs. These advantages in energy saving profoundly points a new research direction in the design of the novel building materials in terms of both fundamental science and architectural engineering.

Funding sources

National Science Foundation Grants CMMI-1635089 and EEC-1343568.

Acknowledgment

We acknowledge the financial support from the National Science Foundation Grants CMMI-1635089 and EEC-1343568.

References

[1] ARPA-E. Single-pan highly insulating efficient lucid designs (SHIELD) program overview; 2014. p. 1–13.
[2] Kim MH, Oh CY, Hwang JH, Choi HW, Yang WJ. Thermal performance of the exhausting and the semi-exhausting triple-glazed airflow windows. Int J Energy Res 2006;30(3):177–90.
[3] Eames PC. Vacuum glazing: current performance and future prospects. Vacuum 2008;82(7):717–22.
[4] Chow Ttai, Li C, Lin Z. Innovative solar windows for cooling-demand climate. Sol Energy Mater Sol Cells 2010;94(2):212–20.
[5] Baetens R, Jelle BP, Gustavsen A. Review: aerogel insulation for building applications: a state-of-the-art review. Energy Build 2011;43(4):761–9.
[6] Berardi U. The development of a monolithic aerogel glazed window for an energy retrofitting project. Appl Energy 2015;154:603–15.
[7] Chow TT, Lyu Y. Effect of design configurations on water flow window performance. Sol Energy 2017;155:354–62.
[8] Carlos JS. Optimizing the ventilated double window for solar collection. Sol Energy 2017;150:454–62.
[9] Goia F, Zinzi M, Carnielo E, Serra V. Spectral and angular solar properties of a PCM-filled double glazing unit. Energy Build 2015;87:302–12.
[10] Wang J, Beltran L. A method of energy simulation for dynamic building envelopes. In: ASHRAE and IBPSA-USA SimBuild 2016, building performance modeling conference; 2016. p. 298–303.
[11] Khodasevych IE, Wang L, Mitchell A, Rosengarten G. Micro-and nanostructured surfaces for selective solar absorption. Adv Opt Mater 2015;3(7):852–81.
[12] Tiwari A, Mishra YK, Kobayashi H, Turner APF. Intelligent nanomaterials. John Wiley & Sons; 2016.
[13] Runnerstrom EL, Llordés A, Lounis SD, Milliron DJ. Nanostructured electrochromic smart windows: traditional materials and NIR-selective plasmonic nanocrystals. Chem Commun 2014;50(73):10555–72.
[14] Ye H, Meng X, Long L, Xu B. The route to a perfect window. Renew Energy 2013;55:448–55.
[15] Mccluney R. Fenestration solar gain analysis. In: FSEC-GP-65 report by Florida Solar Energy Center/University of Central Florida; 1996.
[16] Farley KMJ, Veitch JA. A room with a view: a review of the effects of windows on work and well-being; 2001, No. March, 33.
[17] Aries MBC, Aarts MPJ, Van Hoof J. Daylight and health: a review of the evidence and consequences for the built environment. Lighting Res Technol 2013(47January 2016):6–27.
[18] Boyce P, Hunter C, Howlett O. The benefits of daylight through windows. Lighting Res Center 2003;1(1):1–88.
[19] Ihm P, Nemri A, Krarti M. Estimation of lighting energy savings from daylighting. Build Environ 2009;44(3):509–14.
[20] Hee WJ, Alghoul MA, Bakhtyar B, Elayeb O, Shameri MA, Alrubaih MS, Sopian K. The role of window glazing on daylighting and energy saving in buildings. Renew

Sustain Energy Rev 2015;42:323–43.
[21] Cuce E, Cuce PM. Vacuum glazing for highly insulating windows: recent developments and future prospects. Renew Sustain Energy Rev 2016;54:1345–57.
[22] Loonen R, Hensen JLM, Smart windows with dynamic spectral selectivity–a scoping study. In: Proc building simulation, vol. 15; 2015. p. 8.
[23] Powell MJ, Quesada-Cabrera R, Taylor A, Teixeira D, Papakonstantinou I, Palgrave RG, et al. Intelligent multifunctional $VO_2/SiO_2/TiO_2$ coatings for self-cleaning energy-saving window panels. Chem Mater 2016;28(5):1369–76.
[24] Granqvist CG. Transparent conductors as solar energy materials: a panoramic review. Solar Energy Mater Sol Cells 2007;91(17):1529–98.
[25] Valkonen E, Karlsson B, Ribbing CG. Solar optical properties of thin films of Cu, Ag, Au, Cr, Fe Co Ni and Al. Sol Energy 1984;32(2):211–22.
[26] Martín-Palma RJ. Commentary: spectrally selective coatings on glass: solar-control and low-emissivity coatings. J Nanophotonics 2009;3(1):30305.
[27] Sahu DR, Lin S-Y, Huang J-L. ZnO/Ag/ZnO multilayer films for the application of a very low resistance transparent electrode. Appl Surf Sci 2006;252(20):7509–14.
[28] Yu S, Li L, Lyu X, Zhang W. Preparation and investigation of nano-thick FTO/Ag/FTO multilayer transparent electrodes with high figure of merit. Sci Rep 2016;6.
[29] Kulczyk-Malecka J, Kelly PJ, West G, Clarke GCB, Ridealgh JA, Almtoft KP, et al. Investigation of silver diffusion in $TiO_2/Ag/TiO_2$ coatings. Acta Mater 2014;66:396–404.
[30] Ando E, Miyazaki M. Durability of doped zinc oxide/silver/doped zinc oxide low emissivity coatings in humid environment. Thin Solid Films 2008;516(14):4574–7.
[31] Macleod A. Optical interference coatings–yesterday and today. Chinese Opt Lett 2013;11.
[32] Smith G, Gentle A, Arnold M, Cortie M. Nanophotonics-enabled smart windows buildings and wearables. Nanophotonics 2016;5(1):55–73.
[33] Gesheva KA. Thin film optical coatings for effective solar energy utilization: APCVD spectrally selective surfaces and energy control coatings. Nova Science Pub Incorporated; 2007.
[34] Fu JK, Atanassov G, Dai YS, Tan FH, Mo ZQ. Single films and heat mirrors produced by plasma ion assisted deposition. J Non-Cryst Solids 1997;218:403–10.
[35] Selvakumar N, Barshilia HC. Review of physical vapor deposited (PVD) spectrally selective coatings for mid-and high-temperature solar thermal applications. Sol Energy Mater Sol Cells 2012;98:1–23.
[36] Leftheriotis G, Yianoulis P. Characterisation and stability of low-emittance multiple coatings for glazing applications. Sol Energy Mater Sol Cells 1999;58(2):185–97.
[37] Granqvist CG. Applications of transparent conductors to solar energy and energy efficiency. Handbook of transparent conductors. Springer; 2011. p. 353–423.
[38] Optics. https://windows.lbl.gov/software/Optics/optics.html.
[39] Wang J. (Jialiang). Selection of energy efficient windows for hot climates using genetic algorithms optimization. In: In proceedings of PLEA 2016, international conference on passive and low energy architecture 2016: Cities, Buildings, People: Towards Regenerative Environments; Los Angeles; 2016.
[40] Nielsen KH, Orzol DK, Koynov S, Carney S, Hultstein E, Wondraczek L. Large area, low cost anti-reflective coating for solar glasses. Sol Energy Mater Sol Cells 2014;128:283–8.
[41] Yamada Y, Kitamura S, Miura M, Yoshimura K. Improving the optical properties of switchable mirrors based on Mg–Y alloy using antireflection coatings. Sol Energy Mater Sol Cells 2015;141:337–40.
[42] Loka C, Park KR, Lee K-S. Multi-functional $TiO_2/Si/Ag$ (Cr)/TiN X coatings for low-emissivity and hydrophilic applications. Appl Surf Sci 2016;363:439–44.
[43] Sutanto H, Nurhasanah I, Hidayanto E, Wibowo S, Hadiyanto, Nur H, et al. Synthesis and characterization of ZnO: TiO2 nano composites thin films deposited on glass substrate by sol-gel spray coating technique. In: AIP conference proceedings, AIP Publishing, vol. 1699; 2015. p. 40005.
[44] Raut HK, Dinachali SS, Ansah-Antwi KK, Ganesh VA, Ramakrishna S. Fabrication of highly uniform and porous MgF2 Anti-reflective coatings by polymer-based sol-gel processing on large-area glass substrates. Nanotechnology 2013;24(50):505201.
[45] Lu J-H, Luo J-W, Chuang S-R, Chen B-Y. Antireflection coatings with SiO_x–TiO_2 multilayer structures. Jpn J Appl Phys 2014;53(11S):11RA06.
[46] Raut HK, Ganesh VA, Nair AS, Ramakrishna S. Anti-reflective coatings: a critical, in-depth review. Energy Environ Sci 2011;4(10):3779–804.
[47] Carboni M, Carravetta M, Zhang XL, Stulz E. Efficient NIR light blockage with matrix embedded silver nanoprism thin films for energy saving window coating. J Mater Chem C 2016;4(8):1584–8.
[48] Gorgolis G, Karamanis D. Solar energy materials for glazing technologies. Sol Energy Mater Sol Cells 2016;144:559–78.
[49] Hutchins MG. 3 Spectrally selective materials for efficient visible, solar and thermal radiation control. Sol Therm Technol Build: State Art 2014:37.
[50] Abendroth T, Schumm B, Alajlan SA, Almogbel AM, Mäder G, Härtel P, et al. Optical and thermal properties of transparent infrared blocking antimony doped tin oxide thin films. Thin Solid Films 2017;624:152–9.
[51] Liu H, Zeng X, Kong X, Bian S, Chen J. A simple two-step method to fabricate highly transparent ITO/polymer nanocomposite films. Appl Surf Sci 2012;258(22):8564–9.
[52] Xu X, Stevens M, Cortie MB. In situ precipitation of gold nanoparticles onto glass for potential architectural applications. Chem Mater 2004;16(11):2259–66.
[53] Xiao L, Su Y, Ran J, Liu Y, Qiu W, Wu J, et al. First-principles prediction of solar radiation shielding performance for transparent windows of GdB6. J Appl Phys 2016;119(16):164903.
[54] Schelm S, Smith GB. Dilute LaB 6 nanoparticles in polymer as optimized clear solar control glazing. Appl Phys Lett 2003;82(24):4346–8.
[55] Mendelsberg RJ, Garcia G, Milliron DJ. Extracting reliable electronic properties from transmission spectra of indium tin oxide thin films and nanocrystal films by careful application of the Drude theory. J Appl Phys 2012;111(6):63515.
[56] Jiang F, Leong Y-K, Saunders M, Martyniuk M, Faraone L, Keating A, et al. Uniform dispersion of lanthanum hexaboride nanoparticles in a silica thin film: synthesis and optical properties. ACS Appl Mater Interf 2012;4(11):5833–8.
[57] Adachi K, Miratsu M, Asahi T. Absorption and scattering of near-infrared light by dispersed lanthanum hexaboride nanoparticles for solar control filters. J Mater Res 2010;25(3):510–21.
[58] Tang H, Su Y, Hu T, Liu S, Mu S, Xiao L. Synergetic effect of LaB6 and ITO nanoparticles on optical properties and thermal stability of poly (vinylbutyral) nanocomposite films. Appl Phys A 2014;117(4):2127–32.
[59] Machida K, Adachi K. Particle shape inhomogeneity and plasmon-band broadening of solar-control LaB6 nanoparticles. J Appl Phys 2015;118(1):13103.
[60] Yuan Y, Zhang L, Hu L, Wang W, Min G. Size effect of added LaB 6 particles on optical properties of LaB 6/polymer composites. J Solid State Chem 2011;184(12):3364–7.
[61] Garcia G, Buonsanti R, Llordes A, Runnerstrom EL, Bergerud A, Milliron DJ. Near-infrared spectrally selective plasmonic electrochromic thin films. Adv Opt Mater 2013;1(3):215–20.
[62] Llordés A, Garcia G, Gazquez J, Milliron DJ. Tunable near-infrared and visible-light transmittance in nanocrystal-in-glass composites. Nature 2013;500(7462):323–6.
[63] Bayrak Pehlivan İ, Runnerstrom EL, Li S-Y, Niklasson GA, Milliron DJ, Granqvist C-GA. Polymer electrolyte with high luminous transmittance and low solar throughput: polyethyleneimine-lithium bis (trifluoromethylsulfonyl) imide with In_2O_3: Sn Nanocrystals. Appl Phys Lett 2012;100(24):241902.
[64] Korgel BA. Materials science: composite for smarter windows. Nature 2013;500(7462):278–9.
[65] Zhao Y, Sadat ME, Dunn A, Xu H, Chen C-H, Nakasuga W, et al. Photothermal effect on Fe_3O_4 nanoparticles irradiated by white-light for energy-efficient window applications. Sol Energy Mater Sol Cells 2017;161:247–54.
[66] Feng L, Wu L, Qu X. New horizons for diagnostics and therapeutic applications of graphene and graphene oxide. Adv Mater 2013;25(2):168–86.
[67] Huang X, El-Sayed IH, Qian W, El-Sayed MA. Cancer cell imaging and photothermal therapy in the near-infrared region by using gold nanorods. J Am Chem Soc 2006;128(6):2115–20.
[68] Huang X, Jain PK, El-Sayed IH, El-Sayed MA. plasmonic photothermal therapy (PPTT) using gold nanoparticles. Lasers Med Sci 2008;23(3):217.
[69] Johannsen M, Gneveckow U, Taymoorian K, Thiesen B, Waldöfner N, Scholz R, et al. Morbidity and quality of life during thermotherapy using magnetic nanoparticles in locally recurrent prostate cancer: results of a prospective phase I trial. Int J Hyperth 2007;23(3):315–23.
[70] Link S, El-Sayed MA. Optical properties and ultrafast dynamics of metallic nanocrystals. Ann Rev Phys Chem 2003;54(1):331–66.
[71] Peer D, Karp JM, Hong S, Farokhzad OC, Margalit R, Langer R. Nanocarriers as an emerging platform for cancer therapy. Nature Nanotechnol 2007;2(12):751–60.
[72] Yang H-W, Liu H-L, Li M-L, Hsi I-W, Fan C-T, Huang C-Y, et al. Magnetic gold-nanorod/PNIPAAmMA nanoparticles for dual magnetic resonance and photoacoustic imaging and targeted photothermal therapy. Biomaterials 2013;34(22):5651–60.
[73] Yang K, Zhang S, Zhang G, Sun X, Lee S-T, Liu Z. Graphene in mice: ultrahigh in vivo tumor uptake and efficient photothermal therapy. Nano Lett 2010;10(9):3318–23.
[74] Shi D, Sadat ME, Dunn AW, Mast DB. Photo-fluorescent and magnetic properties of iron oxide nanoparticles for biomedical applications. Nanoscale 2015;7(18):8209–32.
[75] Chu M, Pan X, Zhang D, Wu Q, Peng J, Hai W. The therapeutic efficacy of CdTe and CdSe quantum dots for photothermal cancer therapy. Biomaterials 2012;33(29):7071–83.
[76] Chu M, Shao Y, Peng J, Dai X, Li H, Wu Q, et al. Near-infrared laser light mediated cancer therapy by photothermal effect of Fe_3O_4 magnetic nanoparticles. Biomaterials 2013;34(16):4078–88.
[77] Stratton JA. Electromagnetic theory. John Wiley & Sons; 2007.
[78] Sapareto SA, Dewey WC. Thermal dose determination in cancer therapy. Int J Radiat Oncol Biol Phys 1984;10(6):787–800.
[79] Hill RJ, Nadel SJ. Coated glass: applications and markets. BOC Coating Technology; 1999.
[80] Scheffler M, Dressel M, Jourdan M, Adrian H. Extremely slow drude relaxation of correlated electrons. Nature 2005;438(7071):1135–7.
[81] Chan WCW. Bio-applications of nanoparticles vol. 620. Springer Science & Business Media; 2009.
[82] Sadat ME, Kaveh Baghbador M, Dunn AW, Wagner HP, Ewing RC, Zhang J, et al. Photoluminescence and photothermal effect of Fe_3O_4 nanoparticles for medical imaging and therapy. Appl Phys Lett 2014;105(9):91903.
[83] Singh J. Optical properties of condensed matter and applications vol. 6. John Wiley & Sons; 2006.
[84] Ghosh D, Chattopadhyay N. Gold nanoparticles: acceptors for efficient energy transfer from the photoexcited fluorophores. Opt Photon J 2013.
[85] Bankole OM, Nyokong T. Comparative studies on photophysical and optical limiting characterizations of low symmetry phthalocyanine linked to Fe_3O_4-Ag core-shell or hybrid nanoparticles. New J Chem 2016;40(12):10016–27.
[86] Carmody, J. High performance windows and facades: research and development, tools and market transformation. USGBC GreenBuild conference, Chicago, IL, November; 2007.
[87] Philiplaven, MiePlot. http://www.philiplaven.com/mieplot.htm.
[88] Roper DK, Ahn W, Hoepfner M. Microscale heat transfer transduced by surface plasmon resonant gold nanoparticles. J Phys Chem C 2007;111(9):3636–41.
[89] Han X, Deng Z, Yang Z, Wang Y, Zhu H, Chen B, et al. Biomarkerless targeting and photothermal cancer cell killing by surface-electrically-charged superparamagnetic

Fe_3O_4 composite nanoparticles. Nanoscale 2017.
[90] Mbise GW, Le Bellac D, Niklasson GA, Granqvist CG. Angular selective window coatings: theory and experiments. J Phys D Appl Phys 1997;30(15):2103.
[91] Ng MW, Smith GB, Dligatch S. Spectral switching of the preferred transmission direction in absorbing anisotropic composites. J Phys D Appl Phys 1999;28(12):2578–84.
[92] NFRC. NFRC 102-2010: procedure for measuring the steady-state thermal transmittance of fenestration systems. Silver Spring, MD: National Fenestration Rating Council, Inc.; 2010.